Towards Real-Time Stereoscopic Image Rectification for 3D Visualization

Tony Marrero Barroso, Aubrey K. Dunne, John Mallon, Paul F. Whelan

Centre for Image Processing and Analysis, Dublin City University, Ireland
{tony.marrero, aubrey.dunne, john.mallon, paul.whelan}@eeng.dcu.ie

Abstract. This paper describes a method for stereoscopic rectification with geometric distortion minimisation, to generate suitable image pairs for 3D viewing applications. The current state of the art technique is not optimal as it lacks appropriate mathematical constraints. We present a new approach that enforces the same distortion minimisation criterion with more computational efficiency whilst also achieving superior distortion removal. Detailed mathematical expressions have been developed that fully constrain the system to facilitate the use of faster and more accurate non-linear optimisation algorithms. Appropriate rectification transforms can then be defined at speeds suitable for real-time implementations.

Key words: Stereoscopic rectification, stereovision, 3D visualisation, real time, distortion minimisation.

1 Introduction

Image rectification has long been a standard technique to facilitate 3D stereoscopic image viewing and the techniques encompassing stereoscopic 3D image analysis. Rectification creates a simplified configuration where the epipolar lines in the image pair are aligned either vertically or horizontally, and constitutes a vital preprocessing step in the production of 3D stereoscopic imagery. These image pairs create the illusion of depth by providing each eye with a different viewpoint of the same scene. This illusion cannot effectively be generated unless the same objects seen by each eye are at the same vertical height. Such a configuration can only occur when the epipolar lines of the image pair are aligned horizontally thus requiring stereoscopic rectification.

The promise of generating real time high quality stereoscopic images for 3D viewing is the motivation for this work. The specific focus is on unconstrained camera systems where the relative viewpoints between the stereo image pairs are constantly changing and thus a different rectification is required for each image pair. Several situations arise where such a real-time system is needed. Of specific interest is the synthesis of stereoscopic 3D video content from a monocular video sequence, which can be particularly relevant to Augmented Reality (AR) applications. Accurate, distortion free rectification can be applied in any AR system that can already extract the geometry from a monocular video sequence and

knows where/how to overlay the augmented graphics onto the scene, but also wishes to display the information on a 3D display. Such a system will require to rectify the stereo image pairs in real time, and this paper proposes a method that can achieve this.

Rectification involves subjecting the image pair to a different projective transformation (*planar homography*) for each image. The images are warped during the transformation and since the criterion to mathematically constrain these homographies are not unique [1], several distortion effects arise that do not affect the alignment of the epipolar lines but do interfere with obtaining images suitable for 3D viewing. An accurate minimisation strategy is essential due to the high sensitivity of the rectification transforms. A minute variation in any of the transform's entries can cause variations of tens of pixels in the rectifying images which is sufficient to disrupt the 3D viewing experience. This proposed work presents a novel approach to a rectification strategy that achieves geometric distortion minimisation. With a fully constrained system, the developed mathematical relationships allow for the proposed work to achieve greater accuracy than the current state of the art, with significantly lower computational time costs.

1.1 Related Work

The main approaches to stereoscopic rectification can be grouped into plane-based rectification (*Projective*) and line-based rectification (*Polar*). Projective rectification transforms the entire image from one plane to another, whereas polar rectification transforms each epipolar line differently. Projective methods that do not need a full camera matrix use epipolar geometry to define the planar homographies. Works that need the calculation of a fundamental matrix include [1–3]. Others need only point correspondences between the image pairs to obtain the required transformations [4]. A variety of rectification techniques have arisen from the fundamental works that underpin epipolar geometry. What distinguishes many of these derived methods from each other is the metric that is used to define the rectifying transformation. They exploit the non-uniqueness of the rectification theory [1, 5] to define homographies using their own criterion to improve stereo matching and/or visual appearance.

Robert et al. [6] were amongst the pioneers to consider the distortional effects of rectification on stereo images. They reduce the amount of distortion by considering the transformations that best preserve orthogonality about the image centres. Hartley's approach [1] is to find the appropriate homography by minimising the overall disparity (*in both x and y directions*) between the corresponding rectified points of the stereo image pairs. Although these techniques certainly result in rectifications that improve stereo matching, the results may still be visually distorted and thus not suitable for direct stereoscopic 3D visualization.

Loop and Zhang [2] consider a stratified decomposition of the rectification and decompose each homography into projective and affine components. They constrain affine qualities on the homographies to reduce the distortion. However as skew, scale and aspect ratio are invariant to affine transforms, it is unclear that the metric of 'closest to affine' provides the optimal distortion removal for 3D visualization. Isgrò and Trucco's method [7] requires disparity minimisation along the x-axis to generate a unique solution. Similarly to Hartley, it is suitable for 3D reconstruction but this modification of the x-axis disparity can greatly distort the image and affects stereoscopic viewing in cases where original x-axis disparity must be maintained. Gluckman and Nayar [8], consider the effects of resampling that impede both stereo matching and 3D visualization. They seek to minimize both the loss of pixels (*under-sampling*) and the creation of new pixels (*over-sampling*). This is achieved by minimizing the change in the local area of the images during the transformations, by ensuring that the value of the determinant of the resulting transformation's Jacobian be as close to one as possible.

A method that provides more control over the resampling effects of the rectification transforms is proposed by Mallon and Whelan [3]. Their rectification is a variation on Hartley's method [1], but which also proposes a novel distortion minimisation criterion. By analysing the singular values of each transform's Jacobian, they attempt to maintain the orthogonality and perspective of the original image by defining homographies that result in the Jacobian's two singular values also being as close to one as possible.

1.2 Proposed Approach

This work will only consider uncalibrated projective rectification due to the severe distortions that result from polar rectifications which make the resulting rectified images unsuitable for 3D viewing. Using an uncalibrated rectification technique is preffered as it facilitates a more general implementation for 3D stereo view synthesis. From the various distortion minimisation criterion found in the literature, Mallon and Whelan's [3] adequately addresses the requirements for 3D viewing. In their paper a comparison is made between their method and the two fundamental works of Hartley [1] and Loop and Zhang [2]. Those results show that [3] better preserves the orthogonality and aspect ratio of their rectified images, which are precisely the criterion we currently use to generate the stereoscopic views. They however implement their distortion minimisation with a non-optimal strategy that greatly hinders a real-time application and also affects accuracy. The strategy currently in use is loosely constrained mathematically and thus they are required to use the Nelder-Mead simplex search method to obtain the appropriate terms for their homographies. Nelder-Mead is an unconstrained non-linear minimisation algorithm that is not as efficient as other alternative techniques [9, 10].

The contribution of this work is to implement the distortion removal criteria of [3] in a more accurate and efficient strategy that can enable real-time implementations. To achieve this goal, a detailed study has been conducted into the mathematics of the distortion minimisation process. This in turn has resulted in analytical equations which precisely constrain the system and which enable the use of minimisation algorithms that use exact derivatives in order to converge more efficiently than the Nelder-Mead simplex method.

2 Distortion Minimisation

We propose to modify the distortion minimisation criterion of [3], however the actual epipolar rectification step is adapted from them in its entirety. Their projective homographies are closely derived from Hartley's technique [1], and are solely based on an analysis of the Fundamental matrix ($\mathbf{F}$) which is assumed to be already known. In epipolar rectification the fundamental matrix does not encapsulate any information with regard to the x coordinate of the rectifying homographies ($\mathbf{H}$ *and* $\mathbf{H}'$). In [11] it is demonstrated that the x component of a point is not used by the epipolar constraint. Thus the first row of any such rectifying homography is undetermined. This resulting property is utilised in [3], to define unique first rows ($\mathbf{A}$ *and* $\mathbf{A}'$) without invalidating the epipolar rectification constraints while minimising shearing/skewness and aspect/scale distortions in the images. The final image transformations become $\mathbf{K} = \mathbf{AH}$ and $\mathbf{K}' = \mathbf{A}'\mathbf{H}'$, and it is their implication on the image pixels that will be discussed here. The reader is referred to [3] for more details on how to arrive at these homographies.

The resampling effects of the rectification transformation on the image can be quantified by analysing the local area about an image point. The change in local area about a point p_i, is given by the determinant of the Jacobian $\mathbf{J}$ of the transformation of $\mathbf{K}$ upon the point p_i [12]. A more robust approach is performed in [3] by analysing the singular values of $\mathbf{J}$ instead of its determinant.

$$J(K, p_i) = \begin{bmatrix} \frac{\partial \bar{x}_i}{\partial x_i} & \frac{\partial \bar{x}_i}{\partial y_i} \\ \frac{\partial \bar{y}_i}{\partial x_i} & \frac{\partial \bar{y}_i}{\partial y_i} \end{bmatrix} \tag{1}$$

$$\frac{\partial \bar{x}_i}{\partial x_i} = \frac{\mathbf{k_{11}}(k_{32}y_i + k_{33}z_i) - \mathbf{k_{12}}(k_{31}y_i) - k_{13}(k_{31}z_i)}{(k_{31}x_i + k_{32}y_i + k_{33}z_i)^2} \tag{2}$$

$$\frac{\partial \bar{x}_i}{\partial y_i} = \frac{\mathbf{k_{12}}(k_{31}x_i + k_{33}z_i) - \mathbf{k_{11}}(k_{32}y_i) - k_{13}(k_{32}z_i)}{(k_{31}x_i + k_{32}y_i + k_{33}z_i)^2} \tag{3}$$

$$\frac{\partial \bar{y}_i}{\partial x_i} = \frac{k_{21}k_{32}y_i + k_{21}k_{33}z_i - k_{31}k_{22}y_i - k_{31}k_{23}z_i}{(k_{31}x_i + k_{32}y_i + k_{33}z_i)^2} \tag{4}$$

$$\frac{\partial \bar{y}_i}{\partial y_i} = \frac{k_{22}k_{31}x_i + k_{22}k_{33}z_i - k_{32}k_{21}x_i - k_{32}k_{23}z_i}{(k_{31}x_i + k_{32}y_i + k_{33}z_i)^2} \tag{5}$$

Where:

$$\mathbf{k_{11}} = (\mathbf{a_{11}}h_{11} + \mathbf{a_{12}}h_{21}). \qquad \mathbf{k_{12}} = (\mathbf{a_{11}}h_{12} + \mathbf{a_{12}}h_{22}) \tag{6}$$

An ideal transform completely preserves the resampling of the local area about p_i if both singular values are equal to one. Let $\sigma_{1,2}$ be the first and second singular values of the 2×2 Jacobian matrix $\mathbf{J}$. Then a transform resulting in $\sigma_{1,2} > 1$ induces the creation of extra pixels (*over-sampling*), and $\sigma_{1,2} < 1$ results in the loss of pixels due to compression (*under-sampling*), about the local area of the point p_i. Both these effects can impede stereo matching and 3D visualisation. Over-sampling can smooth out image texture that is required for dense stereo matching while under-sampling can cause aliasing and loss of information. To implement the chosen distortion minimisation criterion, one must search for the optimum values of the affine pair a_{11} and a_{12} which result in singular values that are closest to one. This search is done by minimising the cost function in Equation 7 which maintains the orthogonality and perspective of the original image while minimising the resampling effects of the transformation. Equation 7 has been shown to be convex [3], thus facilitating non-linear minimisation algorithms. The parameter a_{13} is an x direction shift and does not affect distortion, thus it is not taken into account during the distortion minimisation step.

$$f(\hat{a}_{11}, \hat{a}_{12}) = \sum_{i=1}^{n} [(\sigma_1 - 1)^2 + (\sigma_2 - 1)^2] \tag{7}$$

3 Developing the Mathematical Constraints

The goal of this proposed work is to develop a more efficient minimisation strategy, one that can utilise exact derivatives contrary to that of [3] which implements the unconstrained Nelder-Mead algorithm and obtains the singular values using SVD algorithms. Recall that the minimisation distortion criterion being used is that of Equation 7. We thus constrain the system by describing a valid mathematical model that relates the singular values of the Jacobian in Equation 1 to the rectification homography $\mathbf{K}$. This enables the search for the unknown parameters of the affine matrix $\mathbf{A}$ that minimises the distortion effects of the rectification. There are several ways to acquire the singular values of a matrix and the method selected needs to be in the form of a mathematical expression. The preferred analytical relationship that was investigated is expressed in Equation 8, where the singular values (σ_i) of $\mathbf{J}$ are related to the square root of the eigenvalues (μ_i) of the matrix $\mathbf{J}^T\mathbf{J}$.

$$\sigma_i = \sqrt{\mu_i(J^T J)} \tag{8}$$

$$J^T J = \begin{bmatrix} \left(\frac{\partial \bar{x}_i}{\partial x_i}\right)^2 + \left(\frac{\partial \bar{y}_i}{\partial x_i}\right)^2 & \left(\frac{\partial \bar{x}_i}{\partial x_i}\frac{\partial \bar{x}_i}{\partial y_i}\right) + \left(\frac{\partial \bar{y}_i}{\partial x_i}\frac{\partial \bar{y}_i}{\partial y_i}\right) \\ \left(\frac{\partial \bar{x}_i}{\partial x_i}\frac{\partial \bar{x}_i}{\partial y_i}\right) + \left(\frac{\partial \bar{y}_i}{\partial x_i}\frac{\partial \bar{y}_i}{\partial y_i}\right) & \left(\frac{\partial \bar{x}_i}{\partial y_i}\right)^2 + \left(\frac{\partial \bar{y}_i}{\partial y_i}\right)^2 \end{bmatrix} = \begin{bmatrix} \alpha & \omega \\ \omega & \beta \end{bmatrix} \tag{9}$$

Substituting Equations 2, 3, 4 and 5 into $\mathbf{J}^T\mathbf{J}$, letting $R_i = (k_{31}x_i + k_{32}y_i + k_{33}z_i)$ and developing the expressions leads to:

$$\alpha = \frac{1}{R^4}[\mathbf{k_{11}^2}\alpha_1 + \mathbf{k_{12}^2}\alpha_2 + \mathbf{k_{11}k_{12}}\alpha_3] + \left[\frac{\partial \bar{y}_i}{\partial x_i}\right]^2 \tag{10}$$

$$\beta = \frac{1}{R^4}[\mathbf{k_{11}^2}\beta_1 + \mathbf{k_{12}^2}\beta_2 + \mathbf{k_{11}k_{12}}\beta_3] + \left[\frac{\partial \bar{y}_i}{\partial y_i}\right]^2 \tag{11}$$

$$\omega = \frac{1}{R^4}[\mathbf{k_{11}^2}\omega_1 + \mathbf{k_{12}^2}\omega_2 + \mathbf{k_{11}k_{12}}\omega_3] + \left[\frac{\partial \bar{y}_i}{\partial x_i}\frac{\partial \bar{y}_i}{\partial y_i}\right] \tag{12}$$

Where:

$$\alpha_1 = R_i^2 - 2R_i k_{31} x_i + k_{31}^2 x_i^2. \quad \alpha_2 = k_{31}^2 y_i^2. \quad \alpha_3 = 2k_{31}^2 x_i y_i - 2R_i k_{31} y_i.$$

$$\beta_1 = k_{32}^2 x_i^2. \quad \beta_2 = R_i^2 - 2R_i k_{32} y_i + k_{32}^2 y_i^2. \quad \beta_3 = 2k_{32}^2 x_i y_i - 2R_i k_{32} x_i$$

$$\omega_1 = k_{31}k_{32}x_i^2 - R_i k_{32} x_i \qquad \omega_2 = k_{31}k_{32}y_i^2 - R_i k_{31} y_i$$
$$\omega_3 = R_i^4 - R_i k_{31} x_i - R_i k_{32} y_i + 2k_{31}k_{32}x_i y_i$$

Following on from Equation 8, the eigenvalue characteristic equation of $\mathbf{J}^T\mathbf{J}$ is defined as:

$$\mu^2 + (-\alpha - \beta)\mu + (\alpha\beta - \omega^2) = 0 \tag{13}$$

After solving with the general Quadratic Formula and subtituting into Equation 8, the expression that explicitly relates the rectifying transformation to the singular values thus becomes:

$$\sigma_{1,2} = \sqrt{\frac{1}{2}\left(\alpha + \beta \pm \sqrt{(-\alpha - \beta)^2 - 4(\alpha\beta - \omega^2)}\right)} \tag{14}$$

This is the equation to obtain the singular values of $\mathbf{J}(\mathbf{K}, p_i)$ (*the Jacobian of the transformation*), about the local area of point p_i. It is used in conjunction with the cost function in Equation 7 to perform the non-linear minimisation and acquire k_{11} and k_{12}. The simultaneous Equation 6 then is solved to obtain the unknown parameters of the affine matrix $\mathbf{A}$. Similarly to [3], a vector $\mathbf{P}$ consisting of image points p_i is defined (*arranged into a grid encompassing the entire image*). Singular values for each point p_i are then obtained with Equation 14 so that the error of the cost function can be calculated and summed according to Equation 7. To implement the new minimisation algorithms, partial derivatives of the cost function are then obtained with respect to a_{11} and a_{12}. Depending on which non-linear minimisation is used these derivatives are utilised differently, but all ensure a more efficient and accurate convergence to that of the unconstrained Nelder-Mead simplex search method utilised by the current state of the art rectification implementing the same distortion minimisation criterion.

Since the size of the vector $\mathbf{P}$ directly influences the time required to calculate the cost function of Equation 7, a study was conducted on the effect that the size of $\mathbf{P}$ has on the accuracy of the minimisation. Figure 1(a) displays this analysis and shows that a small number of image points is sufficient. Apart from the quantity of points, the location of these points around the image is also of equal importance, with an optimum configuration being one that arranges these points equally spaced throughout the image.

4 Experimental Results

Using the constraints defined in Equation 14, we implement three non-linear minimisation algorithms and compare them with two state of the art techniques common throughout the research community. The classical techniques of *Gradient Descent*, *Gauss-Newton* and *Levenberg-Marquardt*, are implemented in C++ to achieve optimum performance. These are compared with a numerical Levenberg-Marquardt adaptation in C of the *Minpack* optimisation toolkit [13], and with the Nelder-Mead simplex method of Numerical Recipes in C [9]. The implementated Nelder-Mead fully recreates the method used in [3] in that the singular values for the cost function are also obtained by SVD using algorithms from standard mathematical libraries. Minpack's L-M technique utilises Equation 14, but its derivatives are not required as this version of Minpack performs numerical differentiation. Our algorithms are thus directly compared with the state of the art in [3] (*which is the main objective of this work*), and also compared against Minpack's numerical technique. In this way it is demonstrated that the exact analytical derivatives of the developed constraints provide an improvement in the accuracy and computational efficiency of the minimisation.

4.1 Results Overview

The objective of the experiments is to demonstrate the accuracy and speed of the proposed minimisation techniques and compare them against the Nelder-Mead and Minpack alternatives. Each minimisation algorithm requires an initial estimation for the unknown vector it is estimating, the algorithms will thus converge with varying degrees of speed depending on the distance that the initial estimations are from the required values of the unknown parameters. The accuracies of convergence will depend on the method itself and its inherent settings. The settings for all algorithms have been optimised for this specific task and all tolerances have been set as equal as possible.

To demonstrate and compare the convergent behaviour of each algorithm under equal conditions, only one rectifying homography is minimised. Each algorithm is initiated with varying initial estimations and the accuracy and speed of each convergence are recorded and compared. The summary of the numerical results is shown in Table 1, which presents the mean values of all the performed convergences[1]. The plots of the individual convergence results are shown in Figure 2, while Figure 1(b) compares the entire convergence profiles for only one initial condition. The first row of Figure 2 shows the convergence accuracy results of each algorithm with varying initial conditions. The (x,y) axes represent the values of the initial estimates used for a_{11} and a_{12} in each convergence test. The vertical axis represents the accuracy error of the minimisation once the algorithms have completely converged. The bottom row of Figure 2 compares the computational efficiency of each algorithm. It shows the time taken per convergence under varying initial conditions.

[1] Executed on a 2.40 GHz CPU with 3GB of RAM.

Table 1. Average values for the convergence tests of each algorithm.

Algorithm		Accuracy Error (%)	Cost Function Evaluations	Time (ms)
Gradient Descent	(G-D)	6.125	7	0.065
Gauss-Newton	(G-N)	3.625	17	0.113
Levenberg-Marquardt	(L-M)	4.920	16	0.110
Minpack's L-M		4.180	54	0.141
Nelder-Mead		7.133	60	0.785

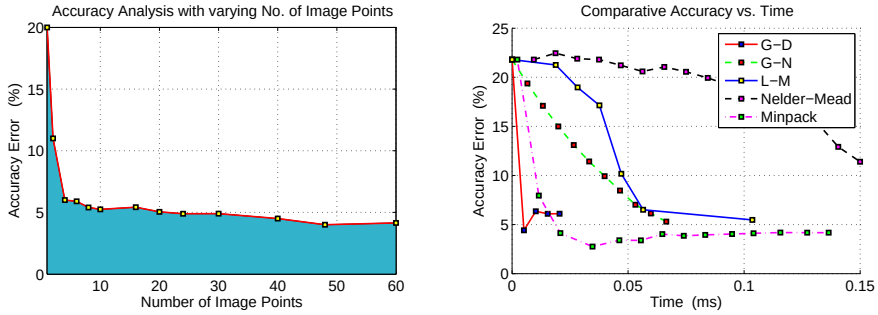

(a) (b)

Fig. 1. (a) Effect of the number of points used by the cost function on the minimisation accuracy; (b) Single comparitive convergence between all the algorithms using the intial conditions of (1,0).

4.2 Discussion

Each algorithm converged to minimum values of approximately 0.7 for a_{11} and 0.1 for a_{12}, having started the estimation from initial estimates ranging from -1.5 to 1.5. It was found that if the values of a_{11} and a_{12} were close to the extremes of the limits chosen, then the resulting homographies would have caused images of size (640x480) to be sheared and distorted by close to 2000 pixels in the horizontal directions. The limits chosen are thus more than sufficient to simulate the bounds that our proposed minimisations will in reality be operating between. Each algorithm proved to be extremely robust since they converged under all conditions.

Table 1 shows the average results of all the convergence tests in order to enable a definitive comparison and see which method is superior under a general set of conditions. Our three proposed algorithms all perform superior under both accuracy and computational efficiency to that of the Nelder-Mead method, thus achieving the desired objective of advancing the current state of the art method. Figure 1(b) illustrates more accurately just how inefficient Nelder-Mead's convergence is compared to the other minimisation approaches.

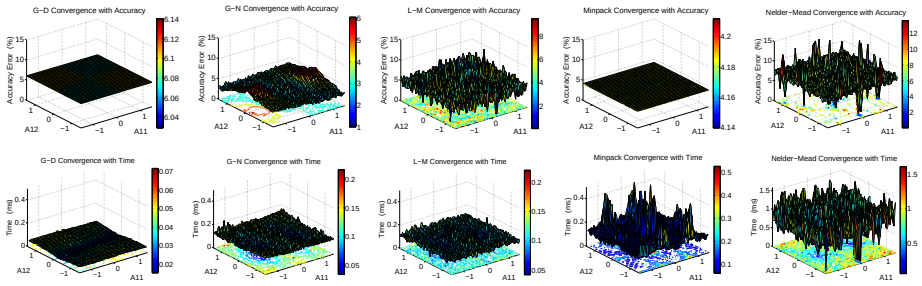

Fig. 2. Accuracy of Convergence for: (1,1)Gradient Descent; (1,2)Gauss-Newton; (1,3)Levenberg-Marquardt; (1,4)Minpack's L-M method; (1,5)Nelder-Mead method. Time of Convergence for: (2,1)Gradient Descent; (2,2)Gauss-Newton; (2,3)Levenberg-Marquardt; (2,4)Minpack's L-M method; (2,5)Nelder-Mead method.

A significant improvement is particularly made in the computational efficiency when the proposed strategy is used, with the Gradient Descent obtaining a mean convergence 12 times faster than that of the mean time of Nelder-Mead, and two times faster than that of Minpack's L-M. Due to the convexity of the cost function [3], a simple algorithm such as the Gradient Descent can still perform exceptionally well compared to the other more robust methods. The mean accuracy errors in Table 1 show that there is minimal accuracy differences between the algorithms and the convergence plots in Figure 2 illustrate that our algorithms converge under all conditions. This validates the mathematical constraints that have been developed and shows the algorithms are robust and converge consistently. Figure 2(1,5) demonstrates that the accuracy of the Nelder-Mead minimisation is more inconsistent and is another reason for why the proposed strategy is superior. Despite Gradient Descent achieving a mean convergence time only twice as fast as that of the Minpack L-M, Gradient Descent's minimum time was 10 times faster than Minpack's minimum. The use of the exact derivatives of the developed mathematical constraints are therefore justifiable considering a difference in accuracy of only 2% between the Gradient Descent and that of the Minpack's L-M. As previously stated, the full range of conditions used in the convergence tests are extreme and are presented solely to convey the robustness of the proposed methods. The bottom row of plots in Figure 2 show that when the given initial estimates are within reasonable bounds of the cost function minima, our proposed methods perform significantly more efficiently than what the averaged data in Table 1 suggests.

5 Conclusion

A new approach has been proposed to achieve the distortion minimisation criterion of Mallon and Whelan [3], and by developing exact mathematical constraints it has enabled the use of a more accurate and computationally efficient strategy. The convergence properties of the proposed model were compared against the

recognised minimisation methods in the field. With the proposed strategy and using the full derivatives of the developed mathematical constraints, a significant computational improvement of a factor of 12 has been obtained. A small improvement in accuracy has also been achieved which ensures a more natural 3D viewing experience. The objectives of this work have therefore been successfully achieved as this strategy advances the current state of the art that implements the same distortion removal criterion. Our strategy can now be used to facilitate systems requiring real-time stereoscopic rectification.

References

1. Hartley, R.: Theory and practice of projective rectification. International Journal of Computer Vision **35** (1999) 115–127
2. Loop, C., Zhang, Z.: Computing rectifying homographies for stereo vision. In: Proceedings of the IEEE Computer Society Conference on Computer Vision and Pattern Recognition. Volume 1., Citeseer (1999) 125–131
3. Mallon, J., Whelan, P.: Projective rectification from the fundamental matrix. Image and Vision Computing **23** (2005) 643–650
4. Fusiello, A., Irsara, L.: Quasi-euclidean uncalibrated epipolar rectification. In: Pattern Recognition, 2008. ICPR 2008. 19th International Conference on. (2008) 1–4
5. Hartley, R., Zisserman, A.: Multiple view geometry in computer vision. Cambridge Univ Pr (2003)
6. Robert, L., Zeller, C., Faugeras, O., Herbert, M.: Applications of non-metric vision to some visually-guided robotics tasks. Visual navigation: from biological systems to unmanned ground vehicles **2** (1997)
7. Isgrò, F., Trucco, E.: Projective rectification without epipolar geometry. In: cvpr, Published by the IEEE Computer Society (1999) 1094
8. Gluckman, J., Nayar, S.: Rectifying transformations that minimize resampling effects. In: IEEE Computer Society Conference on Computer Vision and Pattern Recognition. Volume 1., Citeseer (2001)
9. Press, W., Teukolsky, S., Vetterling, W., Flannery, B.: Numerical recipes: the art of scientific computing. Cambridge Univ Pr (2007)
10. Walter, E., Pronzato, L.: Identification of parametric models. Springer Heidelberg (1997)
11. Weng, J., Ahuja, N., Huang, T.: Optimal motion and structure estimation. IEEE Transactions on Pattern Analysis and Machine Intelligence (1993) 864–884
12. Arnold, V.: Mathematical methods of classical mechanics. Springer-Verlag (1989)
13. Bond, C.: Minpack in c. http://www.crbond.com/download/cmp.zip (2001)